Journal of Electroceramics (2018) 41:73–79
https://doi.org/10.1007/s10832-018-0161-y

Dielectric and piezoelectric properties of $Bi_{1/2}Na_{1/2}TiO_3$–$SrTiO_3$ lead–free ceramics

Trang An Duong[1] · Hyoung-Su Han[1] · Young-Hwan Hong[1] · Young-Seok Park[1] · Hoang Thien Khoi Nguyen[1] · Thi Hinh Dinh[1] · Jae-Shin Lee[1]

Received: 12 December 2017 / Accepted: 20 September 2018 / Published online: 26 September 2018

Abstract
This study investigated the microstructure, crystal structure, and electrical properties of $(1-x)Bi_{1/2}Na_{1/2}TiO_3$–$xSrTiO_3$ (BNST100x; $x = 0.20$, 0.22, 0.24, 0.26, 0.28, and 0.30) lead−free piezoceramics. The average grain size of BNST100x ceramics decreased with increasing $SrTiO_3$ content. A phase transition from nonergodic relaxor (NER) to ergodic relaxor (ER) was observed at $x = 0.26$, and the highest unipolar strain under 4 kV/mm electric field, of 0.25% ($d_{33}^* \approx 620$ pm/V), was obtained at $x = 0.28$. We found that the BNST26 and BNST28 compositions yielded the competitive advantage of larger strain values under lower operating fields compared with other BNT–based lead–free piezoelectric ceramics. Therefore, we regard these ceramics as promising candidates for actuator applications.

Keywords Lead–free · Piezoelectrics · Relaxor · Incipient piezoelectrics · Ferroelectrics

1 Introduction

Lead–based piezoceramics such as lead zirconate titanate $Pb(Zr,Ti)O_3$ (PZT) are the most widely used in commercial applications [1] because of their excellent performance in sensors and actuators. However, PZT ceramics contain more than 60% lead, which is toxic to humans and harmful to the environment. Accordingly, in the last twenty years there has been a great deal of study on lead–free piezoelectric ceramics as alternatives to PZT [2, 3]. In general, three lead–free piezoceramics systems have shown the most promise: those based upon $BaTiO_3$ (BT), $Bi_{1/2}Na_{1/2}TiO_3$ (BNT), and $K_{1/2}Na_{1/2}NbO_3$ (KNN) [4–10]. Among these, BNT–based ceramics are considered to be a promising candidate for actuator applications owing to their excellent electromechanical strain properties; they demonstrate large electric field–induced strain (EFIS) as incipient piezoceramics; this term refers to the phenomenon whereby materials become macroscopically piezoelectric under an applied electric field [11]. However, such large strain only occurs under strong driving field. Therefore, improving the strain under lower electric field is an urgent issue. One promising material system to address this problem is BNT–$SrTiO_3$ (BNST) ceramics. $SrTiO_3$ (ST) doping was beneficial for improving the piezoelectric properties of BNT ceramics [12–14], and can reduce their remanent polarization, yielding relaxor behavior in all compositions [15]. To investigate the morphotropic phase boundary (MPB) in this system, Krauss et al. [15] completed the phase diagram over the entire composition range of $(1-x)Bi_{1/2}Na_{1/2}TiO_3$–$xSrTiO_3$ (BNST100x, from $x = 0$ to $x = 1$) and found that the large strain observed for the ST doping content of $x = 0.25$, which gave the maximum strain of 0.29% under the electric field of 6 kV/mm, supported the hypothesis that the reason for large strain was a field–induced antiferroelectric–ferroelectric phase transition. Besides, a phase boundary between rhombohedral ferroelectric and pseudocubic paraelectric phases was found in the vicinity of BNST28, accompanied by a large strain (~0.19%) under low electric field [16]. On the other hand, it has been reported that a large normalized strain (d_{33}^*) of about 600 pm/V under low electric field for BNST25 ceramics was ascribed to the core–shell structure in recent reports [17, 18].

In the present work, we investigated the microstructure, crystal structure, and electrical properties of $(1-x)Bi_{1/2}Na_{1/2}TiO_3$–$xSrTiO_3$ (BNST100x) in the range of ST doping x between 0.20 and 0.30. We found that the phase transition from nonergodic relaxor (NER) to ergodic relaxor (ER) occurred at $x = 0.26$, and observed the highest strain

✉ Hyoung-Su Han
hsejs@ulsan.ac.kr

[1] School of Materials Science and Engineering, University of Ulsan, 93, Daehak–ro, Nam–gu, Ulsan, Republic of Korea

under 4 kV/mm, of 0.25% ($d_{33}^{*} \approx 620$ pm/V), at the composition $x = 0.28$.

2 Experimental procedure

Specimens of $(1–x)Bi_{1/2}Na_{1/2}TiO_3–xSrTiO_3$ (BNST100x) lead–free piezoceramics with ST doping in the range of 0.20–0.30 were prepared by means of a conventional solid–state reaction method. The component oxide and carbonate powders, Bi_2O_3 (99.9%), TiO_2 (99.0%), Na_2CO_3 (99.8%), and $SrCO_3$ (99.0%), were used as raw materials (High Purity Chemicals, Japan). For each composition, the raw materials were mixed in stoichiometric proportions by means of conventional ball–milling in ethanol using zirconia balls, then dried and calcined at 850 °C for 2 h to form uniform solid solutions. The resultant powders were mixed with polyvinyl alcohol (PVA) binder and then pressed into green body discs of diameter 12 mm under the uniaxial pressure of 98 MPa. Finally, the discs were placed in a sealed alumina crucible and sintered at 1175 °C for 2 h.

The densities of sintered samples were determined using the Archimedes method. Polished and thermally etched sample surfaces were imaged via field–emission scanning electron microscopy (FE–SEM, JEOL JSM–65OFF, Japan) and crystal structures were characterized by means of X–ray diffractometry (XRD, RAD III, Rigaku, Japan). To allow electrical measurements, silver paste was screen printed onto both sides of each specimen, and then burnt in at 700 °C for 30 min. The piezoelectric charge coefficient d_{33} was measured using a piezo d_{33}/d_{31} meter (ZJ–6B; Institute of Acoustics, Chinese Academy of Sciences, Beijing, China). The temperature–dependent dielectric constant and dielectric loss were recorded by using a high temperature electric prober system (KEYSIGHT–E4980AL Precision LCR Meter). Electric field–induced strain and ferroelectric hysteresis loops were measured in a silicon oil bath using a linear variable differential transducer (LVDT) and a modified Sawyer–Tower circuit, respectively.

3 Results and discussion

Surface images of polished and thermally etched BNST100x ceramics are displayed in Fig. 1. All images revealed dense microstructures, and the relative densities reached values of over 96%. The average grain size decreased with increasing ST content. Altering the ST content strongly affected the microstructures of the BNT ceramics, with changes similar to results in the microstructure of ST–modified BNT ceramics reported by Krauss et al. [15]. In fact, these microstructural changes are closely related to the thermodynamic behaviors of the synthesized materials. The formations of BNT and ST phases are known to begin at temperatures over 530 and 560 °C, respectively [19, 20]. Besides, more recently, Koruza et al. [21] reported that temperatures of 587 and 795 °C are required to form BNT and ST phases, based upon Fourier transform infrared (FT–IR) spectrometry, thermogravimetric analysis (TGA), and differential thermal analysis (DTA). This may affect the decreasing grain size with increasing the ST doping level. The largest average grain size was 4.5 μm for BNST20, and the smallest grain size was 2.6 μm for BNST30. In addition, two different surface such as a rough (marked with circle) and smooth (marked with arrow) were detected at all samples. It can be suggested that the rough surface is originated from the domain structure. In fact, the domain structure can be visible by thermal or chemical etching with SEM analysis. 90°, 180°, and Herringbone domain patterns in $BaTiO_3$ [22] and $(K_{0.5}Na_{0.5})NbO_3$–based ceramics [23] as normal ferroelectrics were successfully demonstrated by chemical etching with SEM analysis. In the case of relaxor materials, there is a good example that is associated with the comparative study on domain structure between nonergodic relaxor and ferroelectrics of PLZT ceramics [24], despite those

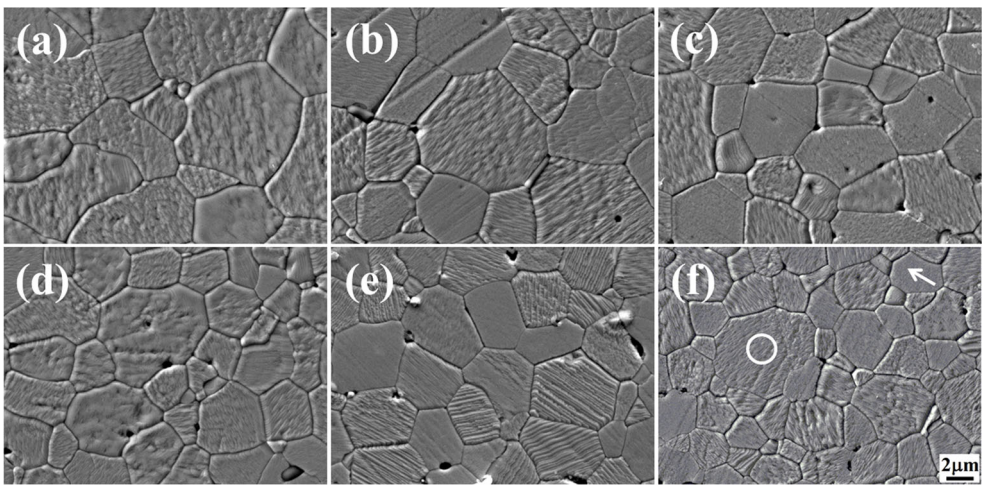

Fig. 1 Polished and thermally etched surface images of BNST100x ceramics with x of **a** 0.20, **b** 0.22, **c** 0.24, **d** 0.26, **e** 0.28, and **f** 0.30

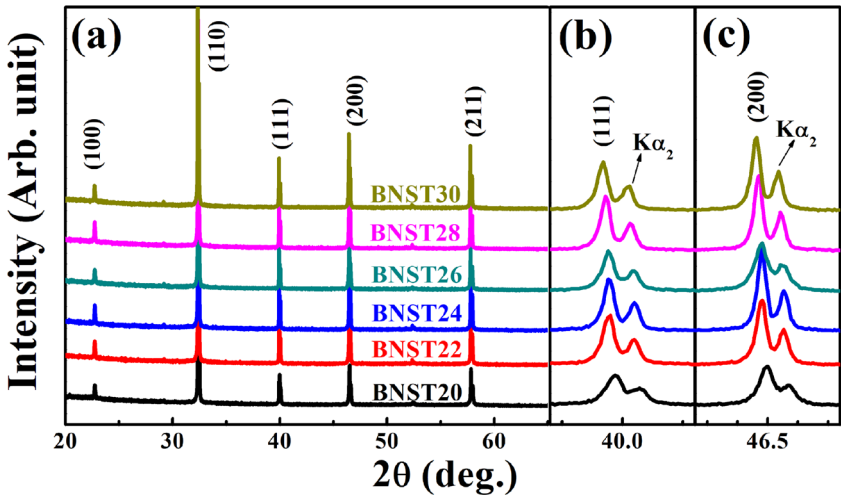

Fig. 2 X–ray diffraction patterns of BNST100*x* ceramics at 2θ of **a** 20–65°, **b** around 40.0°, and **c** around 46.5°

kinds of studies are relatively less than ferroelectric materials. Besides, our research group has successfully demonstrated the domain structure of $Bi_{1/2}(Na,K)_{1/2}TiO_3$ (BNKT)–based relaxor materials by using piezoresponse force microscopy [25]. However, it seems to be difficult to entirey address this appoach in this study because the observed domain structures between ferroelectrics (90°, 180°, and Herringbone domain patterns) and relaxor (nano-sized domain) in literatures were clearly different. Therefore, it is suggested that the advanced analyses such as piezoresponse force microscopy and tansmission electron mcroscopy are required for further clarifying the domain structure.

Figure 2 presents XRD patterns of BNST100*x* ceramics, collected at room temperature. Each sample exhibited a single perovskite phase, indicating the formation of a uniform solid solution without any secondary phase. The peaks around 40.0° and 46.5° were assigned to the (111) and (200) reflections of the cubic crystal structure. Secondary peaks were identified as Kα_2 peaks (Fig. 2b and c). In fact, these Kα_2 as secondary peaks are easily evaluated by Bragg equation and are usually detected at slightly higher 2θ position for main peaks because the used Kα_2 (λ = 1.5444 Å) wavelength is longer than Kα_1 (λ = 1.5406 Å) as X–ray source (Copper). Besides, (111) and (200) peaks were monotonically shifted to low angle with increasing the ST content, meaning that the lattice parameters were increased. The reason for this change is that an ionic radius of the added Sr^{2+} (1.44 Å) is bigger than averaged A–site ionic radii of BNT (Bi^{3+} = 1.36 Å and Na^{1+} = 1.39 Å) [12]. This result indicates that altering the ST content has little effect on the phase transition in the BNT system, which is similar to the behavior observed in other BNT–based lead–free relaxor materials [25–36].

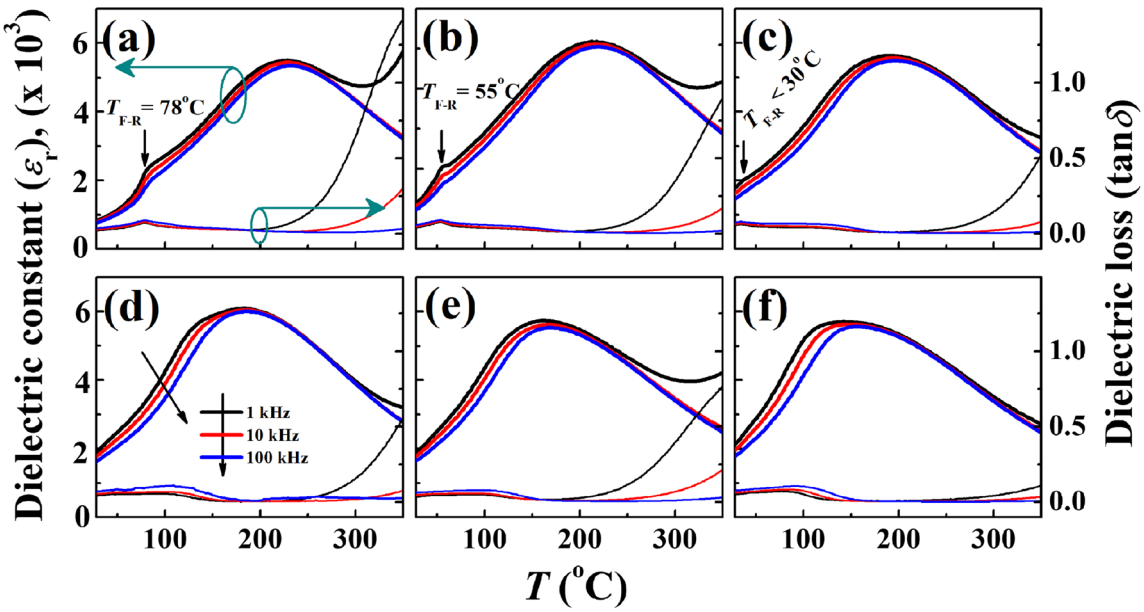

Fig. 3 Temperature dependent dielectric constant (ε_r) and dielectric loss (tanδ) at various frequencies of BNST100*x* ceramics with *x* of **a** 0.20, **b** 0.22, **c** 0.24, **d** 0.26, **e** 0.28, and **f** 0.30

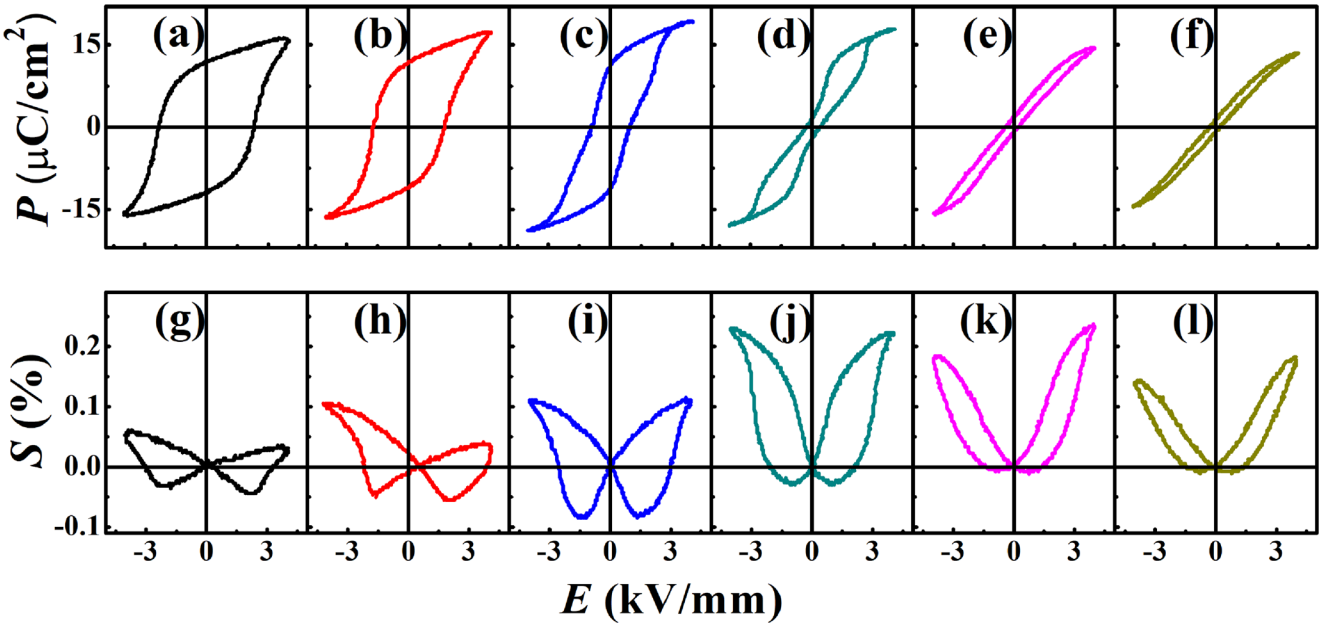

Fig. 4 Polarization (top) and bipolar strain (bottom) curves for BNST100*x* ceramics

Curves of dielectric constant (ε_r) and dielectric loss (tanδ) versus temperature for BNST100*x* ceramics at the different frequencies of 1, 10 and 100 kHz are depicted in Fig. 3. All samples showed strong frequency dispersions at ~100 °C and ~200 °C (the so called dielectric maximum temperature; T_m). In the case of normal ferroelectrics (NFE), the static ε_r exhibits a narrow and a sharp peak at Curie temperature (T_c). Besides, the temperature dependent ε_r of NFE obeys a Curie–Wiess law above T_c and the phase transition of NFE can be thermodynamically first or second order with involving a microscopic symmetry change at T_c [7, 37]. By contrast, the relaxor exhibits a very broad temperature dependence of ε_r peak and strong frequency dispersion near T_m and there is no structural phase transition across T_m [7, 37]. From these points of view, BNST100*x* ceramics can be classified as relaxor. With increasing ST content, T_m and the ferroelectric–to–relaxor transition temperature (T_{F-R}) shifted toward lower temperatures [15, 16, 38, 39]. The T_{F-R} identified for BNST20 and BNST22 were around 78 and 55 °C, respectively, both above room temperature. On the other hand, no transition could be discerned for specimens having $x \geq 0.26$, meaning that the transition of these samples occurred below room temperature. These results imply that a transition from the ferroelectric (or nonergodic relaxor; NER) to relaxor (ergodic relaxor; ER) phases was induced by the change in ST. This is in agreement with various previous studies on BNT–based relaxor materials that have included findings that ferroelectric–to–relaxor transitions can be induced by means of composition modifications [25–35].

Polarization and bipolar strain curves were prepared for the BNST100*x* ceramics in Fig. 4; the BNST20 and BNST22 specimens showed square–shaped polarization curves and the butterfly–shaped strain curves, which are typical ferroelectric features. As discussed above in reference to Fig. 3, the

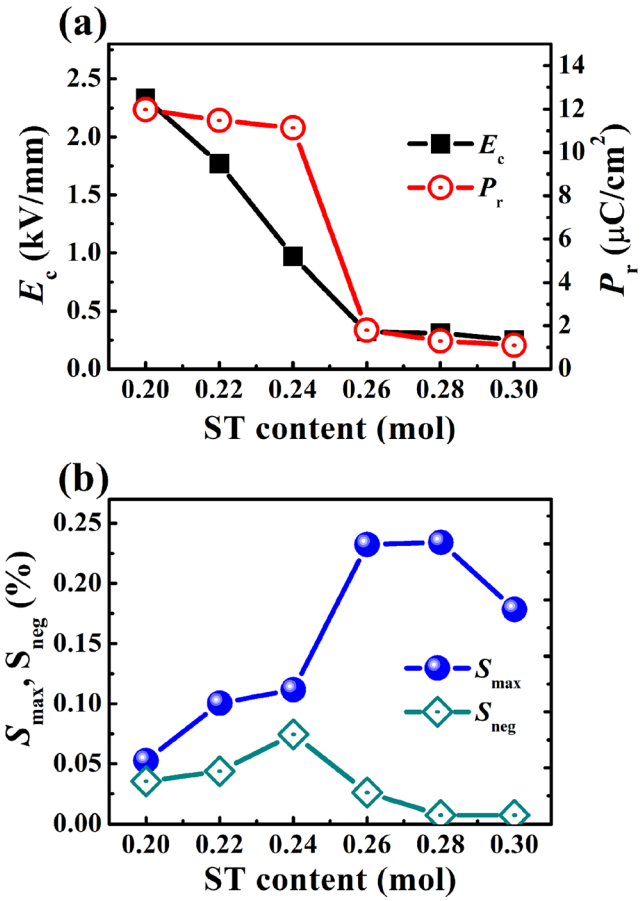

Fig. 5 Characteristic parameters as **a** E_c, P_r and **b** S_{max}, S_{neg} versus ST content of BNST100*x* ceramics under 4 kV/mm electric field

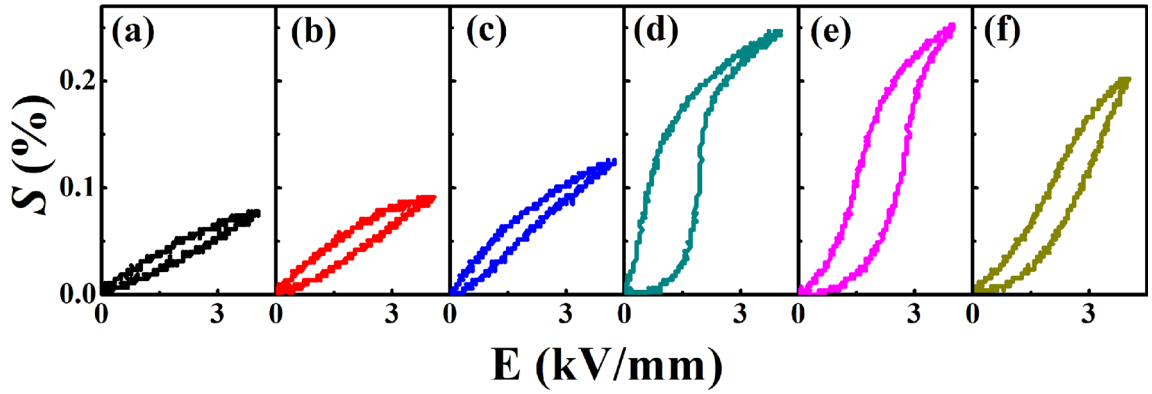

Fig. 6 Electric field–induced unipolar strain curves for BNST100*x* ceramics with *x* of **a** 0.20, **b** 0.22, **c** 0.24, **d** 0.26, **e** 0.28, and **f** 0.30

ferroelectric–to–relaxor transition occurring above room temperature means that both BNST20 and BNST22 ceramics are NER phase at room temperature in the absence of an applied electric field. After electric field is applied to the NER materials, they undergo an irreversible transition to the ferroelectric state. It is well known that the polar region of nanometer size (PNRs) in the relaxor become frozen into a nonergodic state (freezing of the dipole dynamics) [40]. Therefore, the typical ferroelectric features were observed in a polarization as square shape and in a strain as butterfly shape curves for BNST20 and BNST22. Weak constricted polarization curves appeared in BNST24, which is corresponding to a NER–to–ergodic relaxor (ER) transition step as the intermediate procedure. Two facts gave evidence for this phenomenon. One is that the butterfly–shaped strain curve was observed, with large and deep negative strain (S_{neg}). The other is the observation of T_{F-R} at around room temperature (Fig. 3c). On the other hand, double hysteresis curves with large strain were observed for BNST26 ceramics. This large strain can be realized as the consequence of a reduction in negative strain (S_{neg}), coercive field (E_c), and remanent polarization (P_r) as incipient piezoeletrics with ER state [11]. It means that the ER is associated with a reversible electric–field–induced phase transformation into a ferroelectric (FE) because ER is defined as the state of PNRs with randomly distributed direction of dipole moments [40]. Therefore, BNST26 ceramics can be phenomenologically categorized into incipient piezoceramics [11] with ER state. In fact, such large strains have also been observed in other BNT–based relaxor materials, originating from reversible transitions [25–34]. However, further increases in ST concentration led to electrostriction, with zero S_{neg}.

For better understanding of the effects of varying the ST content of BNST ceramics, the characteristic parameters of E_c, P_r, S_{max}, and S_{neg} were extracted from Fig. 4 as the bipolar strain curves; these are plotted in Fig. 5. The values of S_{max} increased with increasing *x* from 0.20 to 0.28, and then decreased with further increases in *x*. BNST28 showed the highest S_{max} under the applied electric field of 4 kV/mm, namely 0.23%. A drastic increase in S_{max} under a modification of ST content means that the nonergodicity or the long–range ordered ferroelectricity has decreased. In fact, this behavior was strongly supported by observed decreases in S_{neg}, E_c, and P_r in Fig. 5a and b, which generally have a trade–off relation in BNT–based relaxor materials.

Unipolar strain curves and its normalized strain (d_{33}^*) were displayed in Figs. 6 and 7. A similar trend in unipolar strain with increasing ST content was observed as shown in bipolar strain. The highest normalized strain value of 625 pm/V was observed for BNST28 ceramics. However, the piezoelectric constant d_{33} revealed a different trend with increasing ST content. As discussed above in reference to Figs. 3 and 4, it is thought that the presence of the electric–field–induced long range ordered ferroelectric (NER) state is responsible for the different trend of d_{33} for BNST100*x* ceramics. d_{33} of 125 pC/N as the highest value was measured at BNST22 ceramics, then drastically decreased with increasing ST content. This implies destabilization of ferroelectricity at zero electric field as ER while the unipolar strain was extremely increased by the applied electric field. Such phenomena have been observed in other BNT–based relaxor materials [25–34].

To confirm the achievements of the present study, the characteristic parameters of maximum strain (S_{max}), applied electric field (E_{max}), and normalized strain (d_{33}^*) were extracted

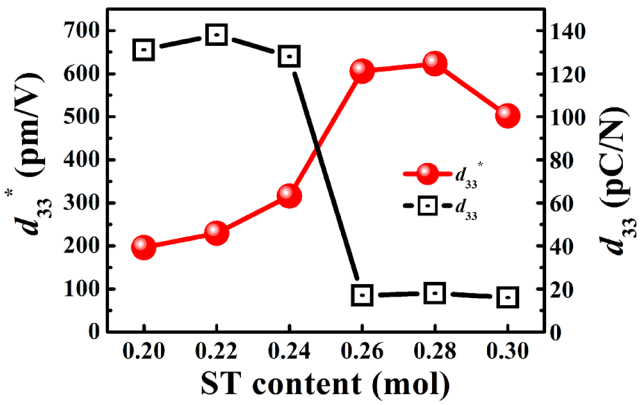

Fig. 7 Normalized strain (d_{33}^*) under 4 kV/mm field and piezoelectric constant (d_{33}) values versus ST content of BNST100*x* ceramics

Table 1 Comparison of normalized strains d_{33}^* (S_{max}/E_{max}) among various lead–free piezoelectric materials. Compositions are abbreviated as follows: $0.74Bi_{1/2}Na_{1/2}TiO_3$–$0.26SrTiO_3$, (BNST26 as this work); $0.72Bi_{1/2}Na_{1/2}TiO_3$–$0.28SrTiO_3$, (BNST28 as this work); $0.72Bi_{1/2}Na_{1/2}TiO_3$–$0.28SrTiO_3$, (BNT–ST28) [16]; $0.75Bi_{1/2}Na_{1/2}TiO_3$–$0.25SrTiO_3$, (25ST) [17]; $0.95[0.8(Bi_{1/2}Na_{1/2})TiO_3$–$0.2(Bi_{1/2}K_{1/2})TiO_3]$–$0.05SrTiO_3$, (BNT–BKT–ST5) [41]; $0.92Bi_{0.5}Na_{0.5}TiO_3$–$0.06BaTiO_3$–$0.02K_{0.5}Na_{0.5}NbO_3$, (BNT–BT–KNN2) [42]; $0.96Bi_{1/2}(Na_{0.84}K_{0.16})_{1/2}(Ti_{0.9825}Nb_{0.0175})O_3$–$0.04SrTiO_3$, (BNKTN–ST) [43]; $0.93Bi_{0.5}(Na_{0.75}K_{0.25})_{0.5}TiO_3$–$0.07BiAlO_3$/$(Bi_{0.5}Na_{0.5})TiO_3$ ceramic composites, (0.93BNKT–0.07BA/BNT) [44]; $0.94Bi_{0.5}(Na_{0.75}K_{0.25})_{0.5}TiO_3$–$0.06BiAlO_3$/$(Bi_{0.5}Na_{0.5})TiO_3$ ceramic composites, (94BNKT–6BA/BNT) [45]; $0.98(Bi_{0.5}Na_{0.39}K_{0.11})TiO_3$–$0.02LaFeO_3$/$(Bi_{0.5}Na_{0.41}K_{0.09})(Ti_{0.985}Sn_{0.015})O_3$ ceramic composites, (2LF/1.5Sn) [46]; $0.96Bi_{0.5}(Na_{0.78}K_{0.22})_{0.5}TiO_3$–$0.04Bi(Mg_{0.5}Ti_{0.5})O_3$/$(Bi_{0.5}Na_{0.5})TiO_3$ ceramic composites, (BNKT–0.04BMT/1.0BNT and BNKT–0.04BMT/1.5BNT) [47]

Material	S_{max} (%)	E_{max} (kV/mm)	d_{33}^* (pm/V)	Reference
BNST26	0.247	4	618	This work
BNST28	0.25	4	625	This work
BNT–ST28	0.29	6	488	[16]
25ST	0.24	4	600	[17]
BNT–BKT–ST5	0.36	6	600	[41]
BNT–BT–KNN2	0.45	8	560	[42]
BNKTN–ST	0.438	5	876	[43]
0.93BNKT–0.07BA/BNT	0.29	4	725	[44]*
94BNKT–6BA/BNT	0.372	4	930	[45]*
2LF/1.5Sn	0.298	4	745	[46]*
BNKT–0.04BMT/1.0BNT	0.254	3.5	725	[47]*
BNKT–0.04BMT/1.5BNT	0.14	2.5	560	

* Ceramic composites

and calculated from Figs. 6 and 7, and then compared with those of other BNT–based lead–free piezoceramics as listed in Table 1. The d_{33}^* values of the previously reported ceramics $0.95[0.8(Bi_{1/2}Na_{1/2})TiO_3$–$0.2(Bi_{1/2}K_{1/2})TiO_3]$–$0.05SrTiO_3$ (BNT–BKT–ST5 [41], $0.92Bi_{0.5}Na_{0.5}TiO_3$–$0.06BaTiO_3$–$0.02K_{0.5}Na_{0.5}NbO_3$ (BNT–BT–KNN2) [42], and $0.72Bi_{1/2}Na_{1/2}TiO_3$–$0.28SrTiO_3$ (BNT–ST28) [16] were 600, 560, and 488 pm/V, respectively. However, relatively strong electric fields (~ 6 or 8 kV/mm as E_{max}) were required to realize these values, which is an urgent issue for BNT–based ceramics as mentioned above. On the other hand, the E_{max} can be decreased to 4 kV/mm with high d_{33}^* performance by forming ceramic/ceramic composites, as listed in Table 1 [44–47]. In fact, this approach seems to be a good method to reduce the E_{max} of BNT–based ceramics, but it has the problem that the fabrication process is quite complex [44–47]. From this point of view, the currently investigated BNST26 and BNST28 lead–free piezoelectric ceramics appear to be good candidates as materials that offer high strain under low operating electric field. Therefore, we believe that these ceramics are promising candidates for actuator applications.

4 Conclusions

$(1–x)Bi_{1/2}Na_{1/2}TiO_3$–$xSrTiO_3$ (BNST100x, $x = 0.20$, 0.22, 0.24, 0.26, 0.28, and 0.30) lead–free piezoceramics were prepared by means of a solid–state reaction. Each specimen showed a single perovskite phase with cubic structure. The average grain size decreased with increasing ST doping. The behavior of these piezoceramics' transitions from nonergodic relaxor (NER) to ergodic relaxor (ER) phases was investigated by studying the temperature dependence of dielectric and electrical properties. The phase transition from NER to ER occurred at $x = 0.26$, and the highest strain under 4 kV/mm electric field, of 0.25% ($d_{33}^* \approx 620$ pm/V), was observed at $x = 0.28$. These results imply that the BNST26 and BNST28 ceramics have the competitive advantage of larger strain under lower operating field compared with other BNT–based lead–free piezoelectric ceramics. Therefore, we regard these ceramics as promising candidates for actuator applications.

Acknowledgements This study was supported by the National Research Foundation (NRF) Grant (2016R1D1A3B01008169) and the Strategic Core Materials Development Program, contract no. G01201311010111, funded by the Ministry of Trade, Industry, and Energy, Republic of Korea. H.S. Han acknowledges the financial support from the National Research Foundation (NRF) Grant (2016R1C1B1014365).

References

1. B. Jaffe, W.R. Cook, H. Jaffe, *Piezoelectric ceramics* (Academic Press, London, 1971)
2. J. Rödel, K.G. Webber, R. Dittmer, W. Jo, M. Kimura, D. Damjanovic, J. Eur. Ceram. Soc. **35**(6), 1659–1681 (2015)
3. C.H. Hong, H.P. Kim, B.Y. Choi, H.S. Han, J.S. Son, C.W. Ahn, W. Jo, J. Materiomics **2**, 1-24 (2016)

4. W. Liu, X. Ren, Phys. Rev. Lett. **103**(25), 257602 (2009)
5. J.F. Li, K. Wang, F.Y. Zhu, L.Q. Cheng, F.Z. Yao, D.J. Green, J. Am. Ceram. Soc. **96**(12), 3677–3696 (2013)
6. J. Wu, D. Xiao, J. Zhu. Chem. Rev. **115**(7), 2559–2595 (2015)
7. C.W. Ahn, C.H. Hong, B.Y. Choi, H.S. Han, Y.H. Hwang, K. Wang, J.F. Li, W. Kim, W. Jo, J. Korean Phys. Soc. **68**(12), 1481–1494 (2016)
8. H.P. Kim, C.W. Ahn, Y. Hwang, H.Y. Lee, W. Jo, J. Korean Ceram. Soc. **54**(2), 86–95 (2017)
9. M. Acosta, N. Novak, V. Rojas, S Patel, R. Vaish, J. Koruza, G.A. Rossetti Jr, J. Rödel, Appl. Phys. Rev. **4**, 041305 (2017)
10. T. Zheng, H. Wu, Y. Yuan, X. Lv, Q. Li, T. Men, C. Zhao, D. Xiao, J. Wu, K. Wang, J.F. Li, Y. Gu, J. Zhu, S.J. Pennycook, Energy Environ. Sci. **10**(2), 528–537 (2017)
11. W. Jo, R. Dittmer, M. Acosta, J. Zang, C. Groh, E. Sapper, K. Wang, J. Rödel, J. Electroceram. **29**(1), 71–93 (2012)
12. Y. Watanabe, Y. Hiruma, H. Nagata, T. Takenaka, Ceram. Int. **34**(4), 761–764 (2008)
13. B. Parija, S.K. Rout, L.S. Cavalcante, A.Z. Simões, S. Panigrahi, E. Longo, N.C. Batista, Appl. Phys. A: Mater. Sci. Process. **109**, 715–723 (2012)
14. D. Lin, K.W. Kwok, H.L.W. Chan, J. Alloys Compd. **481**(1-2), 310–315 (2009)
15. W. Krauss, D. Schütz, F.A. Mautner, A. Feteira, K. Reichmann, J. Eur. Ceram. Soc. **30**(8), 1827–1832 (2010)
16. Y. Hiruma, Y. Imai, Y. Watanabe, H. Nagata, T. Takenaka, Appl. Phy. Lett. **92**(26), 262904 (2008)
17. M. Acosta, W. Jo, J. Rödel, J. Am. Ceram. Soc. **97**(6), 1937–1943 (2014)
18. M. Acosta, L.A. Schmitt, L.M. Luna, M.C. Scherrer, M. Brilz, K.G. Webber, M. Deluca, H.J. Kleebe, J. Rödel, W. Donner, J. Am. Ceram. Soc. **98**(11), 3405–3422 (2015)
19. T. Kainz, M. Naderer, D. Schütz, O. Fruhwirth, F.A. Mautner, K. Reichmann, J. Eur. Ceram. Soc. **34**(15), 3685–3697 (2014)
20. H. Tagawa, K. Kimura, T. Fujino, K. Ouchi, D. Kagaku, J. Electrochem. Soc. Jpn. **52**, 154-159 (1984)
21. J. Koruza, V. Rojas, L.M. Luna, U. Kunz, M. Duerrschnabel, H.J. Kleebe, M. Acosta, J. Eur. Ceram. Soc. **36**(4), 1009–1016 (2016)
22. Y. Tan, J. Zhang, Y. Wu, C, Wang, V. Koval, B. Shi, H. Ye, R. McKinnon, G. Viola, H. Yan. Sci. Rep. **5**, 9953 (2015)
23. F. Azough, M. Wegrzyn, R. Freer, S. Sharma, D. Hall, J. Eur. Ceram. Soc. **31**(4), 569–576 (2011)
24. M. Otonicar, A. Reichmann, K. Reichmann, J. Eur. Ceram. Soc. **36**(10), 2495–2504 (2016)
25. T.H. Dinh, J.K. Kang, J.S. Lee, N.H. Khansur, J. Daniels, H.Y. Lee, F.Z. Yao, K. Wang, J.F. Li, H.S. Han, W. Jo, J. Eur. Ceram. Soc. **36**(14), 3401–3407 (2016)
26. H.S. Han, W. Jo, J.K. Kang, C.W. Ahn, I.W. Kim, K.K. Ahn, J.S. Lee, J. Appl. Phys. **113**(15), 154102 (2013)
27. W. Jo, S. Schaab, E. Sapper, L.A. Schmitt, H.J. Kleebe, A.J. Bell, J. Rödel, J. Appl. Phys. **110**(7), 074106 (2011)
28. N. Chen, W. Yao, C. Liang, S. Xiao, J. Hao, Z. Xu, R. Chu, Ceram. Int. **42**(8), 9660–9666 (2016)
29. V.D.N. Tran, A. Ullah, T.H. Dinh, J.S. Lee, J. Electron. Mater. **45**, 2639-2643 (2016)
30. P. Jarupoom, P. Jaita, R. Yimnirun, G. Rujijanagul, D.P. Cann, Curr. Appl. Phy. **15**(11), 1521–1528 (2015)
31. L. Wang, T.K. Song, S.C. Lee, J.H. Cho, Y.S. Sung, M.H. Kim, K.S. Choi, Curr. Appl. Phy. **10**(4), 1059–1061 (2010)
32. N.B. Do, H.B. Lee, D.T. Le, S.K. Jeong, I.W. Kim, W.P. Tai, J.S. Lee, Curr. Appl. Phy. **11**(3), S134–S137 (2011)
33. A. Ullah, C.W. Ahn, A. Hussain, S.Y. Lee, H.J. Lee, I.W. Kim, Curr. Appl. Phy. **10**(4), 1174–1181 (2010)
34. A. Ullah, C.W. Ahn, A. Hussain, I.W. Kim, Curr. Appl. Phy. **10**(6), 1367–1371 (2010)
35. C.H. Lee, H.S. Han, T.A. Duong, T.H. Dinh, C.W. Ahn, J. S. Lee. Ceram. Int. **43**(14), 11071–11077 (2017)
36. H.S. Han, D.J. Heo, T.H. Dinh, C.H. Lee, J.K. Kang, C.W. Ahn, V.D.N. Tran, J.S. Lee, Ceram. Int. **43**(10), 7516–7521 (2017)
37. G.A. Samara, J. Phys. Condens. Matter **15**(9), R367–R411 (2003)
38. M. Chandrasekhar, P. Kumar, J. Electroceram. **38**(1), 111–118 (2017)
39. H.H. Su, C.S. Hong, C.C. Tsai, S.Y. Chu, ECS J. Solid State Sci. Technol. **5**(10), N67–N71 (2016)
40. A.A. Bokov, Z.E. Ye, J. Mater. Sci. **41**(1), 31–52 (2006)
41. K. Wang, A. Hussain, W. Jo, J. Rödel, J. Am. Ceram. Soc. **95**(7), 2241–2247 (2012)
42. S.T. Zhang, A.B. Kounga, E. Aulbach, H. Ehrenberg, J. Rödel, Appl. Phys. Lett. **91**(11), 112906 (2007)
43. R.A. Malik, J.K. Kang, A. Hussain, C.W. Ahn, H.S. Han, J.S. Lee, Appl. Phys. Express **7**(6), 061502 (2014)
44. D.S. Lee, D.H. Lim, M.S. Kim, K.H. Kim, S.J. Jeong, Appl. Phys. Lett. **99**, 062906 (2011)
45. D.S. Lee, S.J. Jeong, M.S. Kim, K.H. Kim, Jpn. J. Appl. Phys. **52**, 021801 (2013)
46. T.H. Dinh, J.K. Kang, H.T.K. Nguyen, T.A. Duong, J.S. Lee, V.D.N. Tran, K.N. Pham, J. Kor. Phys. Soc. **68**(12), 1439–1444 (2016)
47. A. Khaliqa, M. Sheeraz, A. Ullahb, J.S. Lee, C.W. Ahn, I.W. Kim, Sens. Actuators A Phys. **258**, 174–181 (2017)